OPTIMIZATION AND ANALYSIS OF LIFTING EFFICIENCY FOR POWER CATWALK UNDER MULTI-CONSTRAINT CONDITIONS

PENG WU * [1]

To enhance the lifting efficiency of power catwalk operations and determine the optimal hydraulic cylinder diameter selection, this study focuses on shape optimization of the front lifting manipulator. The hydraulic cylinder diameters investigated range from Φ160mm to Φ320mm, with incremental steps of 20mm and 30mm. Considering the inherent uncertainty in multi-boundary constraints, a mechanical model is established under both local and global coordinate systems. Additionally, an optimization function is developed using C language to address the quantification of uncertain constraint boundaries. Through systematic optimization, the proposed method identifies the optimal installation position and hydraulic cylinder diameter selection. The results demonstrate that the selected cylinder not only meets the operational requirements for lifting tasks but also operates at near-maximum capacity while maintaining excellent expansion efficiency. These findings provide valuable insights and reference frameworks for similar optimization design tasks in hydraulic system applications.

Keywords: power catwalk, lifting efficiency, multi-constraint conditions, structural optimization

1. Introduction

Currently, power catwalks for drilling rigs are primarily categorized into three configurations: fixed, lifting, and grabbing. Among these, the lifting power catwalk stands out due to its ability to elevate drill strings from ground level to the height of the drilling table. This configuration effectively mitigates potential damage to drill strings that may occur with fixed power catwalks and offers superior safety and reliability compared to grabbing power catwalks.

Based on the classification of lifting mechanisms, two primary types of lifting power catwalks are distinguished:

(1) Winch-traction type [1-2]: This type relies on steel wire ropes or hinges for lifting operations. Its advantages include a simple structural design and high operational efficiency. However, the inherent flexibility of steel wire ropes

* Corresponding author

[1] Senior engineer, Qingdao military-civilian integration development promotion center, Qingdao, China, e-mail: wupeng-ets@163.com.

or hinges may induce vibrations during the lifting process, potentially affecting stability.

(2) Hydraulic cylinder-driven type [3-5]: This type employs hydraulic cylinders to drive robotic arms for lifting operations. Its key advantage lies in the excellent stability of hydraulic cylinders, ensuring smooth and steady lifting. However, the lifting efficiency of hydraulic cylinders is generally lower than that of winch-traction systems.

Under constant flow rate conditions in the hydraulic system, the installation position and angle of the lifting cylinder directly influence both the lifting force and the lifting stroke. Additionally, hydraulic cylinders of varying specifications exhibit distinct extension/retraction speeds, thrust ranges, and minimum installation requirements. To enhance lifting efficiency, the author conducts shape optimization by treating the hinge point position of the front lifting arm of the hydraulic cylinder-driven power catwalk as an independent variable. This optimization aims to minimize the time required for the power catwalk to position the lifting pipe at the designated location.

This optimization design involves a complex problem with multiple constraints and variables [6-9]. Due to the influence of diverse factors, the constraint boundaries exhibit multi-objective characteristics. In this study, the author focuses on shape optimization of the lifting arm as the foundation, systematically considers the diversity of constraint boundaries, and optimizes the lifting time to identify the optimal solution for improving lifting efficiency. The findings provide a reference framework and practical guidance for similar optimization design tasks in hydraulic systems or related mechanical applications.

2. General scheme

As depicted in Figure 1, the hydraulic cylinder lifting power catwalk employs a four-bar linkage mechanism as its fundamental design. During operation, the separation mechanism attached to the pipe rack guides the pipes into the V-shaped groove located at the center of the transport arm. Subsequently, the front lifting cylinders extend, causing the fore-end of the transport arm to rise and rotate around the rear-end pivot. Once the transport arm reaches the designated angle, the front lifting cylinders are locked in position. Following this, the rear lifting hydraulic cylinders extend to ensure the fore-end of the transport arm aligns smoothly with the drill floor. Finally, the transport trolley advances the pipe toward the wellhead, coordinating with other handling devices such as hoists and top drives to complete the operation.

It is evident that both the front upper lifting arm and the front lower lifting arm can be modeled as a triangular structure defined by three hinge points. By optimizing the geometric configuration of this triangle—including its side lengths

and interior angles—the optimal propulsive force and installation distance for hydraulic cylinders can be determined. Subsequently, through systematic optimization of hydraulic cylinder selection, the shortest pipe lifting time can be achieved.

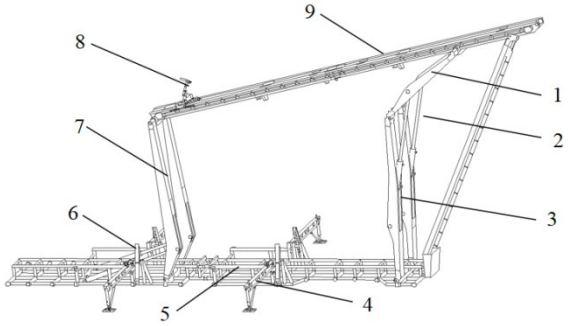

1- Front upper lifting arms; 2- Front lifting hydraulic cylinders; 3- Front lower lifting arms; 4- Substructure; 5- Pipe rack;6- Rear lifting hydraulic cylinders; 7- Rear robotic arms; 8- Transfer trolley; 9- Transfer arm.

Fig.1 Structural schematic diagram of the cylinder lifting power catwalk

3. Model development

3.1 Gravity center of each member under local coordinate system

All components of the power catwalk, including the transfer arm, front upper lifting arm, front lower lifting arm, and front lifting cylinders, can be simplified as structural members as shown in Figure 2. In the figure, points 0, 1, 2, and 3 represent the hinge points of the structure, while points 4 and 5 denote the hinge points connecting to the front lifting cylinders. The variables L_{01}, L_{13}, L_{23} and L_{54} indicate the lengths of the transfer arm, front upper lifting arm, front lower lifting arm, and front lifting cylinder, respectively.

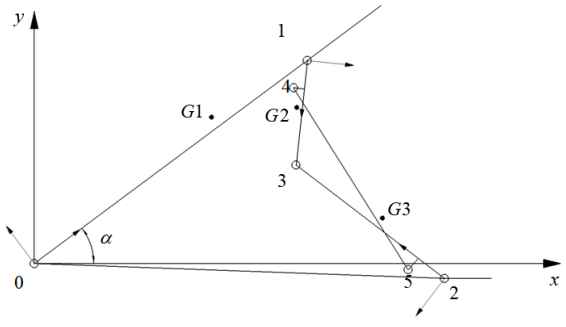

Fig.2 Simplified model of power catwalk as members

A local coordinate system P0 is established with point 0 as the origin, enabling the description of the transfer arm's center of gravity as $G_1(x_{G1}', y_{G1}')$ under P0. Similarly, a local coordinate system P1 is established with point 3 as the origin, allowing the characterization of the front upper lifting arm's center of gravity as $G_2(x_{G2}', y_{G2}')$ under P1. The position of hinge point 4 in the front upper lifting arm structure is variable; therefore, a constraint subset will be established for its horizontal and vertical coordinates. Analogously, a local coordinate system P2 is established with point 2 as the origin, facilitating the description of the front lower lifting arm's center of gravity as $G_3(x_{G3}', y_{G3}')$ under P2. The position of hinge point 5 in the front lower lifting arm structure is also variable, necessitating the establishment of another constraint subset for its horizontal and vertical coordinates, similar to that for hinge point 4. To clearly distinguish variables under local coordinate systems from those under the global coordinate system, a prime symbol " ' " is added to the upper right of variables defined within local coordinate systems.

3.2 Global coordinate system and geometric equations

A global coordinate system is established with joint 0 as the origin. The positions of the other hinge joints are defined within this coordinate system.

$$\begin{cases} x_1 = x_0 + L_{01}\cos\alpha \\ y_1 = y_0 + L_{01}\sin\alpha \end{cases} \tag{1}$$

$$\begin{cases} x_3 = x_2 + L_{23}\cos\theta_{23} \\ y_3 = y_2 + L_{23}\sin\theta_{23} \end{cases} \tag{2}$$

$$\begin{cases} x_4 = x_1 + x_{14}'\cos\theta_{13} - y_{14}'\sin\theta_{13} \\ y_4 = y_1 + x_{14}'\sin\theta_{13} + y_{14}'\cos\theta_{13} \end{cases} \tag{3}$$

$$\begin{cases} x_5 = x_2 + x_{25}'\cos\theta_{23} - y_{25}'\sin\theta_{23} \\ y_5 = y_2 + x_{25}'\sin\theta_{23} + y_{25}'\cos\theta_{23} \end{cases} \tag{4}$$

the gravity centers of each member are defined as follows:

$$\begin{cases} x_{G1} = x_0 + x_{G1}'\cos\theta_{01} - y_{G1}'\sin\theta_{01} \\ y_{G1} = y_0 + x_{G1}'\sin\theta_{01} + y_{G1}'\cos\theta_{01} \end{cases} \tag{5}$$

$$\begin{cases} x_{G2} = x_1 + x_{G2}'\cos\theta_{13} - y_{G2}'\sin\theta_{13} \\ y_{G2} = y_1 + x_{G2}'\sin\theta_{13} + y_{G2}'\cos\theta_{13} \end{cases} \tag{6}$$

$$\begin{cases} x_{G3} = x_2 + x_{G3}'\cos\theta_{23} - y_{G3}'\sin\theta_{23} \\ y_{G3} = y_2 + x_{G3}'\sin\theta_{23} + y_{G3}'\cos\theta_{23} \end{cases} \tag{7}$$

among them, θ_{01}, θ_{13}, θ_{23} and θ_{54} respectively denote the angles between the transfer arm, front upper lifting arm, front lower lifting arm, and front lifting hydraulic cylinders, and the horizontal direction. The trigonometric functions of these angles can be expressed as the ratio of the difference between the horizontal or vertical coordinates and the origin to the distance between the hinge joints and the origin. x_{14}' represents the abscissa of hinge joint 4 within the relative coordinate system P1, while y_{14}' represents the ordinate of hinge joint 4 within P1.

Similar naming conventions apply to other parameters..

3.3 Static equilibrium equations

As shown in Figure 3, R_{0x} denotes the supporting reaction force at hinge joint 0 in the x-direction under the global coordinate system, while R_{0y} denotes the supporting reaction force at hinge joint 0 in the y-direction under the global coordinate system. A similar naming convention applies to the other supporting reaction forces, and further repetition is omitted for brevity.

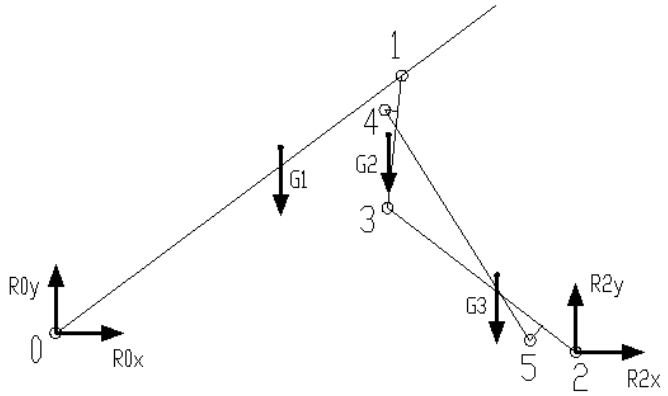

Fig.3 Force diagram for complete member model

For the entire structure, the sum of all forces must satisfy equilibrium conditions in the *x*-direction, which means $\Sigma x = 0$:

$$R_{0x} + R_{2x} = 0 \tag{8}$$

For the entire structure, the sum of all forces must satisfy equilibrium conditions in the *y*-direction, which means $\Sigma y = 0$:

$$R_{0y} + R_{2y} - G_1 - G_2 - G_3 = 0 \tag{9}$$

Regarding the transfer arm, the sum of moments exerted on hinged joint 1 must be zero, which means $\Sigma M(1) = 0$:

$$R_{0x} y_1 - R_{0y} x_1 + G_1 (x_1 - x_{G1}) = 0 \tag{10}$$

When considering the front upper lifting arms, front lower lifting arms, and front lifting hydraulic cylinders as a single system, the sum of moments about hinged joint 1 must be zero. This indicates that $\Sigma M(1) = 0$:

$$R_{2x}(y_1 - y_2) + R_{2y}(x_2 - x_1) - G_2(x_{G2} - x_1) - G_3(x_{G3} - x_1) = 0 \tag{11}$$

Regarding the front lower lifting arms, the sum of moments exerted on joint 3 must be zero, which means $\Sigma M(3) = 0$:

$$F_{54x}(y_3 - y_5) + F_{54y}(x_5 - x_3) + R_{2x}(y_3 - y_2) + R_{2y}(x_2 - x_3) - G_3(x_{G3} - x_3) = 0 \tag{12}$$

By combining equations (1) to (12), the thrust of the front lifting hydraulic cylinders can be calculated as:

$$F_{54} = [G_3(x_{G3} - x_3) - R_{2x}(y_3 - y_2) - R_{2y}(x_2 - x_3)] / [(y_3 - y_5)\cos\theta_{54} + (x_5 - x_3)\sin\theta_{54}] \tag{13}$$

the reaction forces exerted on hinged joint 2 can be deduced as:

$$R_{2x} = \frac{-(x_2 - x_1)\left[G_1 x_{G1} + x_1(G_2 + G_3)\right] + x_1\left[G_2(x_{G2} - x_1) + G_3(x_{G3} - x_1)\right]}{y_1(x_2 - x_1) + x_1(y_1 - y_2)} \tag{14a}$$

$$R_{2y} = \frac{y_1\left[G_2(x_{G2} - x_1) + G_3(x_{G3} - x_1)\right] + (y_1 - y_2)\left[G_1 x_{G1} + x_1(G_2 + G_3)\right]}{y_1(x_2 - x_1) + x_1(y_1 - y_2)} \tag{14b}$$

4. Optimization process

The geometric relationship equations and static equilibrium equations for the hydraulic cylinder lifting power catwalk are formulated as C language programs. Boundary conditions are then implemented to solve the objective functions. Finally, the optimal installation position for the hydraulic cylinders is derived based on the computational results.

4.1 Design variables

As is shown in Table 1, the abscissas of hinge joints 4 and 5 are selected as independent design variables. The installation position of the hydraulic cylinders

is determined by these variables, which directly influence the thrust and stroke of the hydraulic cylinders during the lifting operation.

Table 1

Design variables and symbolic description

Symbol	Type	Explanation
x14	independent variable	the abscissa of joint 4 under the relative coordinate system P1
x25	independent variable	the abscissa of joint 5 under the relative coordinate system P2
F54	dependent variable	the thrust of the front lifting hydraulic cylinders
R0x	dependent variable	the horizontal support reaction force of joint 0 under global coordinate system
R0y	dependent variable	the vertical support reaction force of joint 0 under global coordinate system
L54	dependent variable	the direct distance between the hinged joints 4 and 5
C54	dependent variable	the stroke of front lifting cylinders (difference between the extension length and the initial installation)
t54	dependent variable	The time required for the fore-end of transport arm reaching to designated position
α	independent variable	angle between the transport arm and the horizontal direction

4.2 Objective function

The shape optimization design of the front lifting arms is aimed at improving lifting efficiency. Therefore, the time required for the fore-end of the transfer arm to reach the designated position is selected as the minimization objective function:

$$\min t54\ (x14\ ,\ x25) \tag{15}$$

4.3 Constrained conditions

Table 2

Constraints under different cylinder diameters

Diameters for cylinders	Thrust ranges of the cylinders	Safety distances	Telescoping speeds of hydraulic rods
ϕ160mm	584.1kN≤ F＜656kN	≥507mm	87m/s
ϕ180mm	656kN≤ F＜830kN	≥547mm	68m/s
ϕ200mm	830kN≤ F＜1024kN	≥625mm	55m/s
ϕ220mm	1024kN≤ F＜1240kN	≥645mm	46m/s
ϕ250mm	1240kN≤ F＜1602kN	≥720mm	35m/s
ϕ280mm	1602kN≤ F＜2008kN	≥820mm	28m/s
ϕ300mm	2008kN≤ F＜2306kN	≥880mm	24m/s
ϕ320mm	2306kN≤ F＜2547.9kN	≥950mm	21m/s

Hydraulic cylinders with varying diameters exhibit distinct thrust ranges, installation distances, and strokes. Initially, it is essential to ensure that the hydraulic cylinder thrusts satisfy the lifting requirements of the transfer arm at the initial moment. Subsequently, when addressing the optimization problem for lifting efficiency, the goal is to identify the shortest lifting time. Table 2 presents the constraint conditions, including thrust ranges, safety distances, and extension/retraction speeds of hydraulic rods corresponding to different cylinder diameters. It should be noted that the extension/retraction speeds of hydraulic rods are calculated based on the maximum hydraulic system flow rate of 210 L/min and a design pressure of 207 bar.

Based on the above boundary condition analysis, a constraint arrays Yg[8][5] is defined in C programs:

```
double Yg[8][5]=
{{160,584.1,656,507,87},{180,656,830,547,68},{200,830.0,1024,625,55},{220,1024,1240,645,46},
{250,1240,1620,720,35},{280,1620,2008,820,28},{300,2008,2360,880,24},{320,2306,2547.9,950,12}};
```

4.4 Optimization program

A system of equations is formulated as the WP() function in the C language program, based on the geometric relationship equations and mechanical equilibrium equations (1)-(14) of the hydraulic cylinder lifting power catwalk. The horizontal axis variation range of hinge joint 4 on the front upper lifting arm is discretized into 20 equal intervals, while that of hinge joint 5 on the front lower lifting arm is discretized into 30 equal intervals. A loop structure WP_A() is defined in C to systematically arrange and combine these two sets of data. The values are then input into the WP() function to solve for values of design variables that satisfy the static boundary conditions. The main programs for this loop structure are as follows:

```
for(k=0;k<nk;k++) {
        for(i=0;i<30;i++) {
                x25=x250+x25m*i/29.0;
                for(j=0;j<20;j++) {
                        x14=x140+x14m*j/19.0;    alpha=0.0;    WP();    L540=L54;
                        F540=F54;    R0x0=-R2x;    R0y0=G1+G2+G3-R2y;    alpha=alpham*Ar;
                        WP();    C54=2*L540-L54;    t54=(L54-L540)/Yg[k][4];
                        if(C54>Yg[k][3] && fabs(F540)>=Yg[k][1] && fabs(F540)<=Yg[k][2])
                        fprintf(fp_out,"x14=%f x25=%f F540=%f R0x=%f R0y=%f S=%f t54=%f\n",
                                x14,x25,F540,R0x0,R0y0,C54,t54);
                                }
                        }
                }
```

4.5 Manual selection

Table 3

Optimal solutions of various cylinder diameters

Cylinder Diameter (mm)	Position of Hydraulic Cylinder (mm)		Thrust for Hydraulic Cylinder (kN)	Supporting Reaction Force (kN)		Safety Distance (mm)	Telescoping Time (s)
ϕ180	x14=2595.84	x25=2223.20	F540= -815.89	R0x=529.07	R0y=41.62	S=601.01	t54=37.88
ϕ200	x14=2984.73	x25=3179.89	F540= -974.50	R0x=529.07	R0y=41.62	S=727.38	t54=34.14
ϕ220	x14=3244.00	x25=3897.41	F540= -1117.82	R0x=529.07	R0y=41.62	S=735.69	t54=30.68
ϕ250	x14=3244.00	x25=2821.13	F540= -1247.87	R0x=529.07	R0y=41.62	S=1785.86	t54=40.58

Four sets of cylinder diameters (ϕ180mm, ϕ200mm, ϕ220mm, ϕ250mm) encompass feasible regions totaling 160 variable value sets that satisfy the constraint conditions, as determined by the optimization calculations in the C language programs. As shown in Table 3, the arrays corresponding to the shortest extension/retraction time for each cylinder diameter are manually selected for comparison purposes.

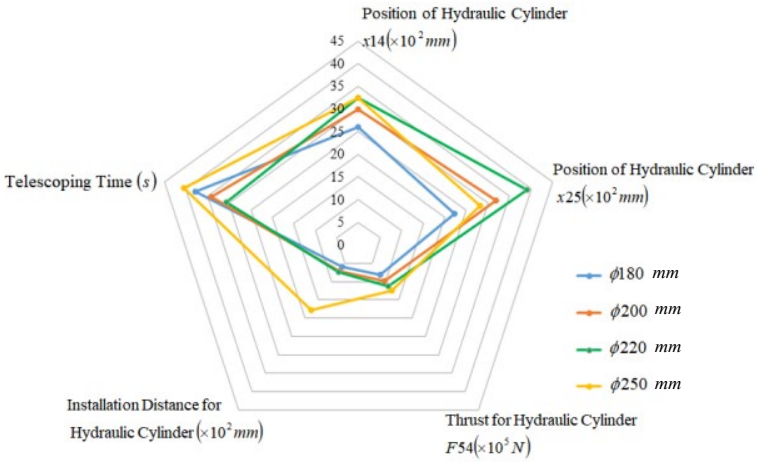

Fig.4 Schematic of optimal solutions under different cylinder diameters

From the radar matrix diagram shown in Fig. 4, it can be concluded that a cylinder diameter of ϕ180mm is the optimal solution for the optimization design.

This conclusion is attributed to the fact that the ϕ250mm cylinder diameter, with a larger installation distance and higher hydraulic cylinder thrust, results in the longest extension/retraction time. Conversely, the ϕ 200mm and ϕ 220mm cylinder diameters, characterized by a greater x14 (abscissa of hinge joint 4 in the local coordinate system), lead to shorter front upper lifting arm lengths and closer proximity between joints 4 and 3. This configuration induces higher local stress in the front upper lifting arms. By comparing the data in Tables 2 and 3, it is evident that the thrust and installation safety distance of the ϕ180mm cylinder diameter nearly reach the limits under the boundary conditions and are close to the self-performance limits. Thus, the ϕ 180mm cylinder diameter offers superior efficiency, utilization, and cost-effectiveness, making it the optimal solution.

5. Simulation Verification

The virtual prototype model of the power catwalk, as shown in Figure 5, is imported into the dynamic simulation software ADAMS.

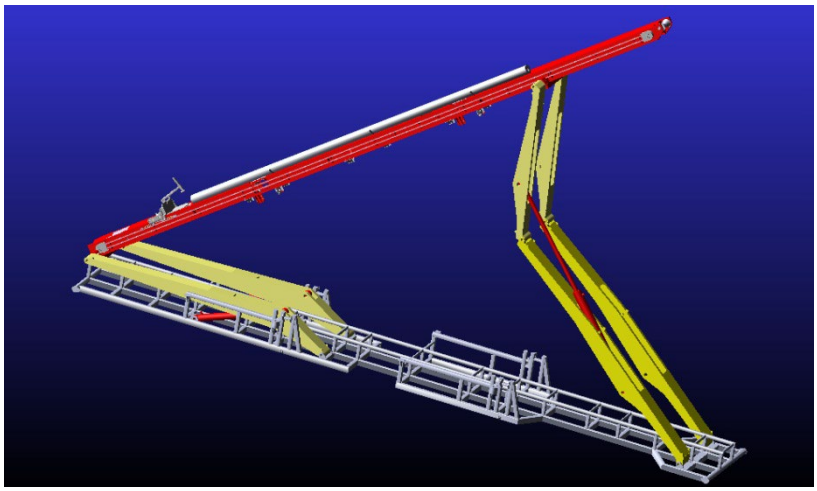

Fig.5 Virtual prototype model of the power catwalk in ADAMS

Subsequently, materials are assigned to each component, and kinematic pairs are established based on the connection relationships between components. Gravity is applied to the system, and the maximum-mass drill collar is positioned within the transport arm's V-shaped groove. The sliding pair between the cylinder barrel and piston rod is designated as the driving pair to simulate the maximum thrust of the front lifting hydraulic cylinders. The sliding speed is set to 68mm/s, with a stroke of 2576mm and a runtime of 38 seconds, ensuring consistency with the results from the preceding chapters. The STEP function (time, 0, 0, 38, 2576) is utilized to simulate the working process of the front lifting hydraulic cylinders.

The relationship curve between the thrust and working time of the front lifting cylinders is shown in Figure 6. The thrust reaches its maximum value of 840 kN at the start of the lifting process and then exhibits an exponential decay. This result aligns with the maximum thrust value of 815.9 kN obtained through C language optimization programs, with a deviation of less than 3%. Therefore, it is concluded that the multi-boundary optimization model for the front lifting arms is valid, the computational results are precise, and the optimization outcomes are reliable.

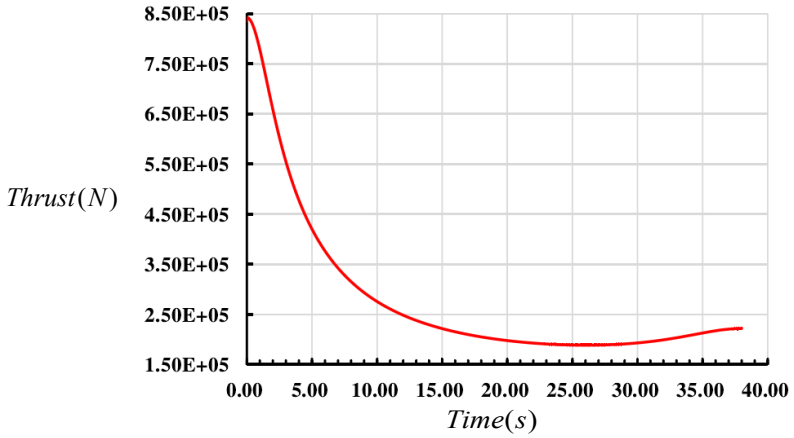

Fig.6 Varying curve of thrust of front lifting cylinder along with working time

6. Conclusions

The front lifting arm of the hydraulic cylinder lifting power catwalk, equipped with eight cylinder diameters (ϕ160mm, ϕ180mm, ϕ200mm, ϕ220mm, ϕ250mm, ϕ280mm, ϕ300mm, and ϕ320mm), is studied as the research object. The installation positions, considering the uncertainty of multiple boundary constraints such as hydraulic cylinder thrust and safety distance, are treated as independent design variables. Based on the geometric and mechanical equilibrium equations of the power catwalk established under both local and global coordinate systems, an optimization function is proposed in the C language. By quantifying the uncertain constraint boundaries and utilizing the optimization function, the optimal installation positions and cylinder type selections are obtained. Under optimal conditions, the hydraulic cylinders meet the lifting operation requirements and maximize their working capacity, achieving a telescoping time of 38 seconds. This optimization result, demonstrating higher efficiency, utilization, and cost-effectiveness, reaches the limitation values under boundary conditions and those of self-performance indicators. Dynamic analysis for verifying the lifting operation process is conducted using ADAMS simulation

software. The comparison reveals a difference of 24.1 kN between the two methods, corresponding to an error of less than 3%, confirming the correctness and reasonableness of the multi-boundary optimization model proposed by the author, with results that are both genuine and reliable.

REFERENCES

[1] *J. Chen, L. Xiong, H.H. Wang, Y. Yang,* Collision Analysis and Motion Control Based on Lift-Type Power Catwalk, Actuators, Vol. **13**, Iss. 12, 2024, DOI: 10.3390/ACT13120494.

[2] *Q. L. Sun, L. He, D. Feng, X. L. Chen, L. L. Ding, Y. L. Tu,* Modeling and analysis of structure parameters on the lifting force for power catwalk, Journal of Engineering, Design and Technology, Vol. **19**, Iss. 1, 2021, DOI: 10.1108/jedt-09-2018-0147.

[3] *T. A.Fang, Z. X. Zhou, C. L. Wu, J. Lv, W. D. Zuo,* Automated Pipe Handling System Suitable for Retrofitting Servicing Rigs in China, International Journal of Oil, Gas and Coal Engineering, Vol. **8**, Iss. 1, 2020, DOI: 10.11648/j.ogce.20200801.12.

[4] *P. Yu, E. C. Jin, S. J. Kang, Y. J. Li,* Design of the Hydraulic System for the Rise-fall Device in Power Catwalk, Advances in Engineering Research, Vol. **103**: Proceedings of the 3rd International Conference on Material Engineering and Application (ICMEA 2016), 2016, DOI: 10.2991/ICMEA-16.2016.79.

[5] *Y. H. Sun, F. Y. Zhang, Q. Y. Wang, K. Gao,* Application of "Crust 1" 10k ultra-deep scientific drilling rig in Songliao Basin Drilling Project (CCSD-SKII), Journal of Petroleum Science and Engineering, Vol. **145**, 2016, http://dx.doi.org/10.1016/j.petrol.2016.04.003.

[6] *X. L. Zhang, B. H. Fan, C. J. Wang,* Optimal design of pneumatic balancing mechanism for power assisted manipulator, U.P.B. Sci. Bull., Series D, Vol. **84**, Iss. 1, 2022.

[7] *Y. Romasevych, V. Loveikin, B. Bakay, I. Rudko,* Optimal tuning of belt conveyor soft-starter via PSO-ROT-RING method, U.P.B. Sci. Bull., Series D, Vol. **85**, Iss. 2, 2023.

[8] *A. Antonov,* Design optimization of a parallel – serial manipulator considering stiffness criteria, Robotics, Vol. **13**, Iss. 12, 2024, DOI: 10.3390/ROBOTICS13120176.

[9] *V. K. Nguyen, H. T. Pham, H. H. Pham, Q. K. Dang, P. S. Minh,* Reliability-based multi-objective optimization design of a compliant feed drive mechanism for micromachining, Applied Sciences, Vol. **13**, Iss. 8, 2023, DOI: 10.3390/APP13084968.